Experience in Using Bmad with the Cornell Electron/positron Storage Ring

– A Selection –

Operations: Virtual CESR (CesrV)

Online optics correction

Particle tracking

Vacuum chamber modeling

Synchrotron radiation

Photon reflectivity (specular and diffuse)

Offline analysis (magnet calibration, alignment, difference kick fitting)

Jim Crittenden
Cornell ERL/EIC Group
Bmad Development Meeting
6 October 2022

CesrV: Example of operations use for orbit correction

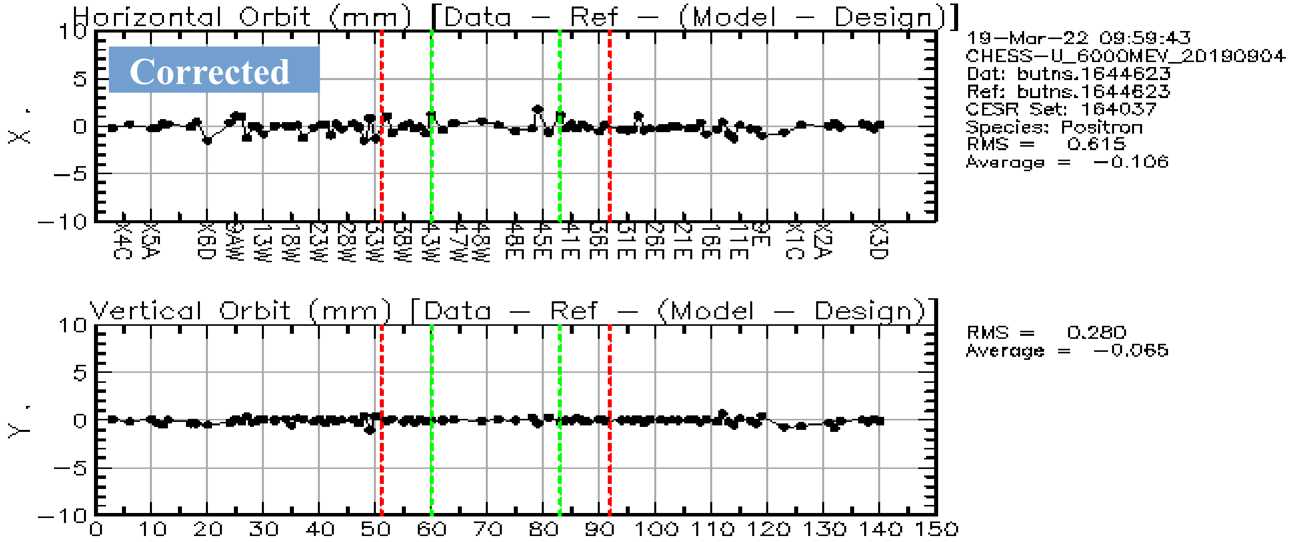

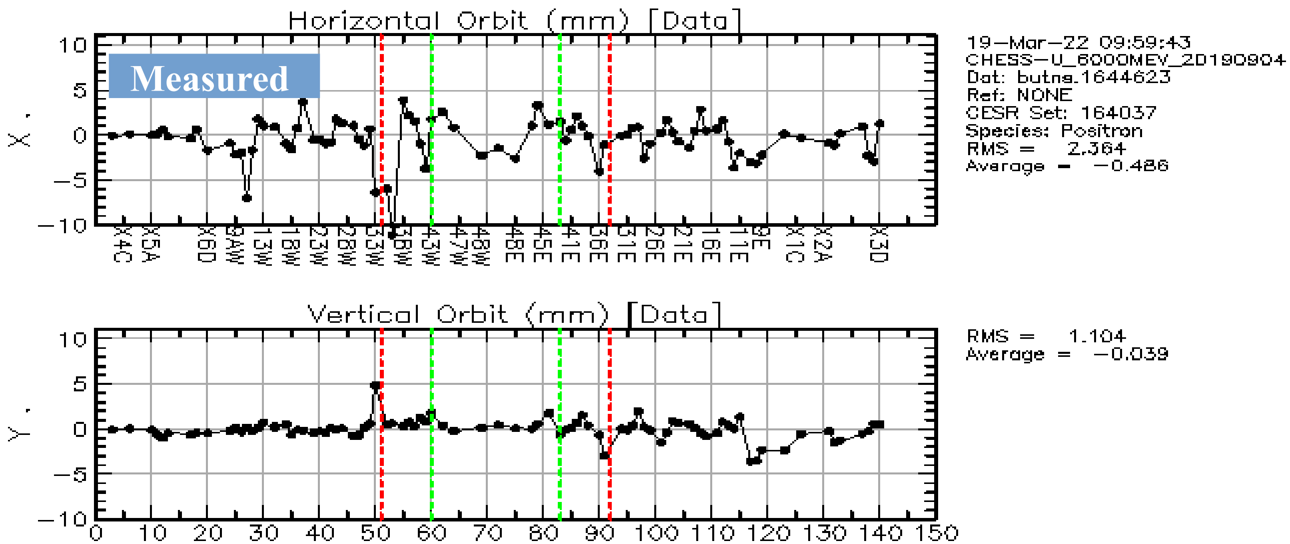

Example of CESR orbit correction using steerings and a measured orbit.

For our experiment we wish to obtain a centered orbit from the operations orbit we inherited.

During startup (today!) we use this procedure to correct phase and coupling as well as the orbit.

For my recent experiments, I have used this optimization procedure offline on recorded phase and orbit difference measurements to obtain the best estimates for the values of dipole and quadrupole kicks at a sextupole where I have changed the K_2 value.

Wave analysis

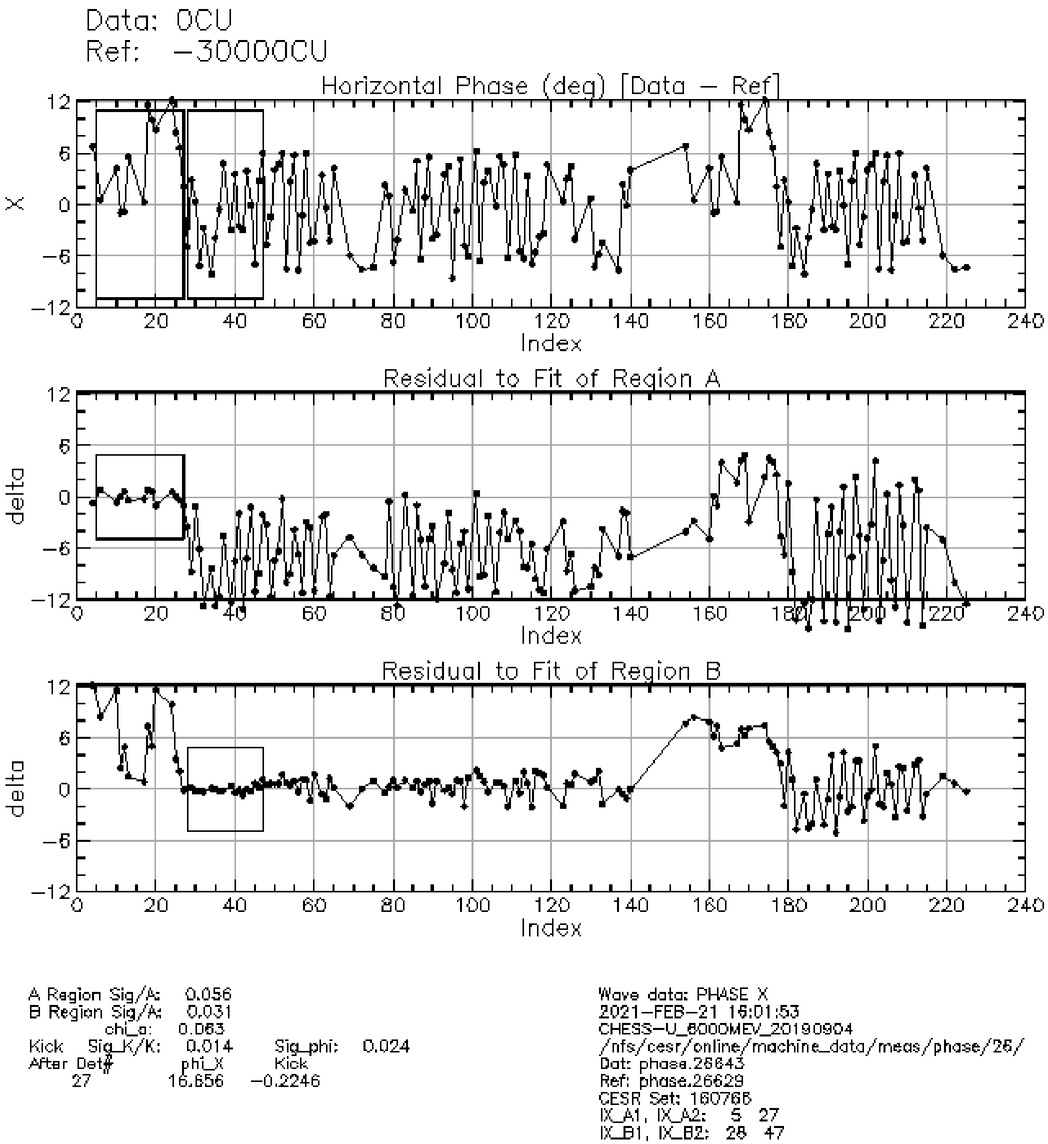

Wave analysis is generally used by the operations group to find the sources of orbit and phase errors.

This example shows my use of it to measure the phase kick produced by changing the strength of a particular sextupole. So the choice of fit range is given by the known location of the sextupole

D. Sagan, *Betatron phase and coupling correction at the Cornell Electron/Positron Storage Ring*, Phys. Rev. ST Accel. Beams 3, p. 102801 (2000).

Detailed model of CESR vacuum chamber

Simulating synchrotron radiation in accelerators including diffuse and specular reflections, G. Dugan and D. Sagan, Phys. Rev. Accel. Beams 20, 020708 (2017)

Plan view

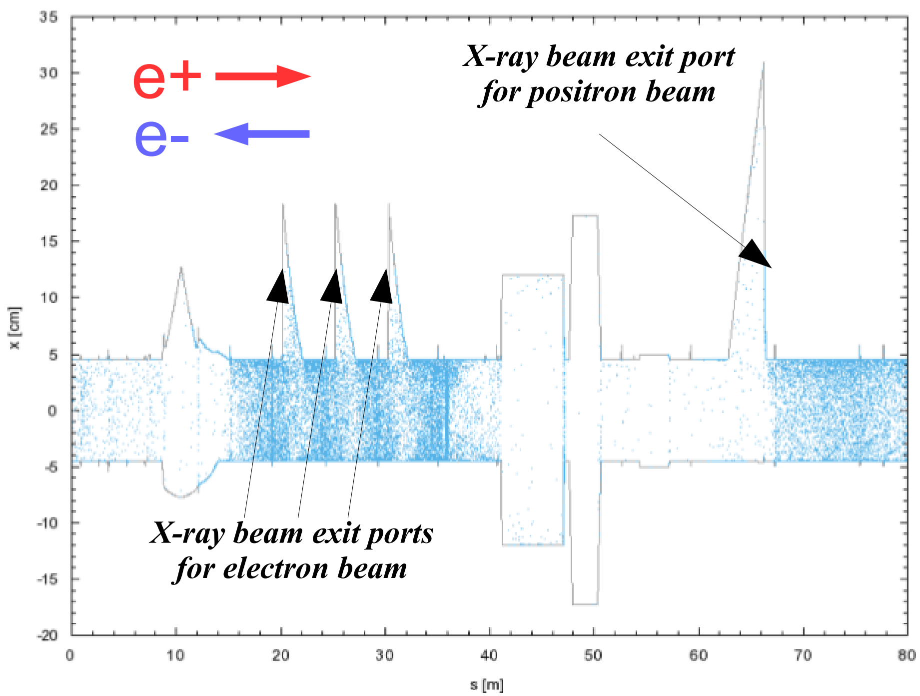

Elevation view

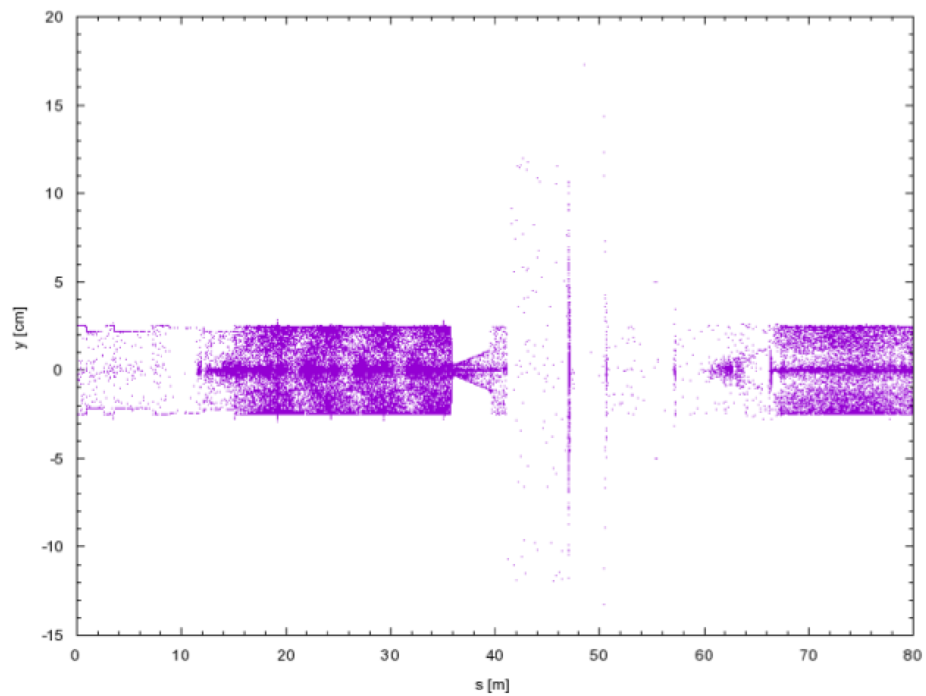

10^6 photons tracked around the 768-m CESR ring
Vacuum chamber model includes gate valves, bellows, etc

Absorbed photon energies and grazing angles 5.3 GeV e+ beam

Photon energies

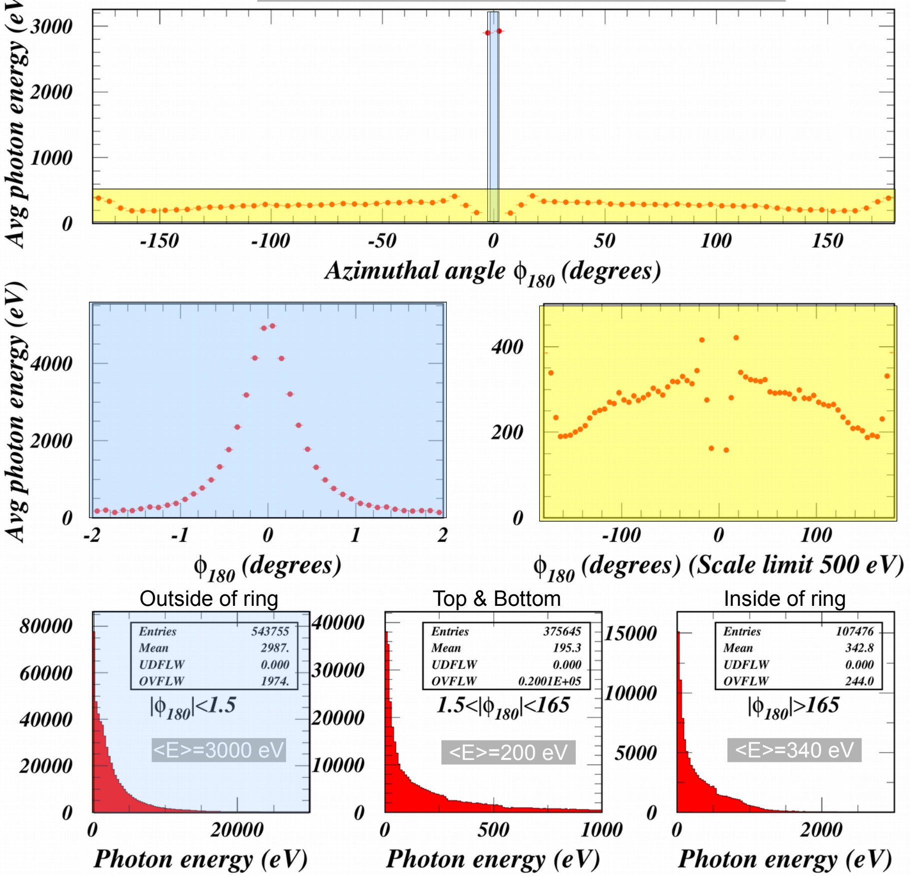

Photon incident angle

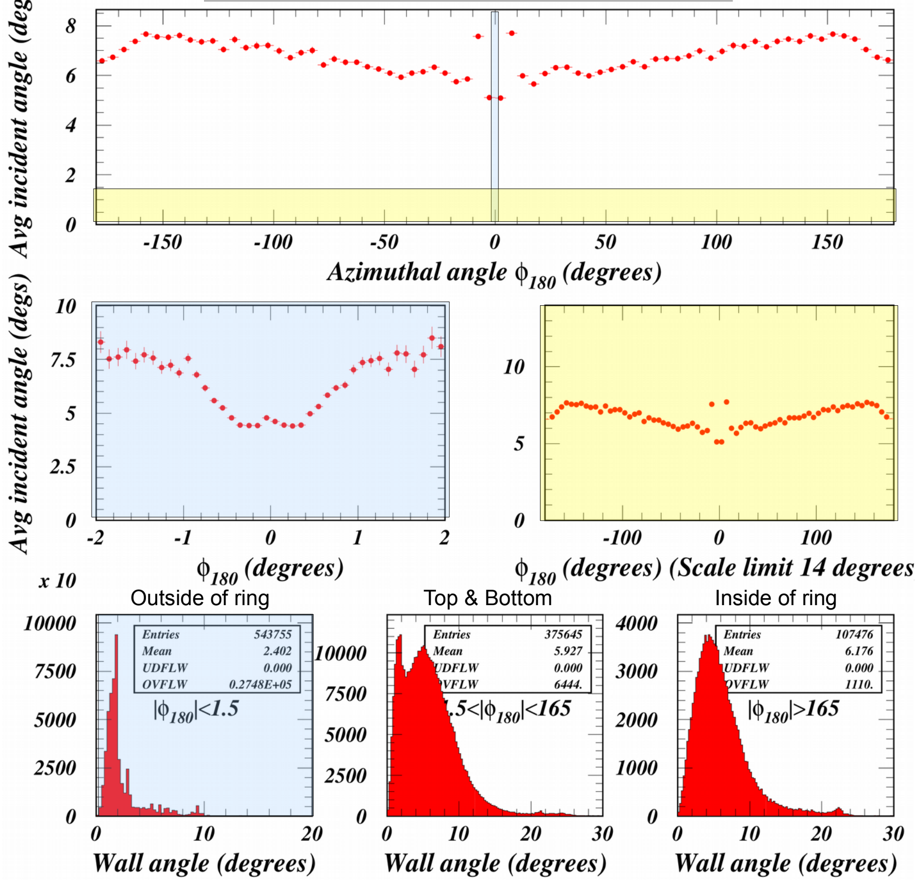

Dramatic dependence of photon energies and incident angles on azimuthal absorption location.
We distinguish three azimuthal regions for generating electron energies .
Absorption site and energy distributions are averaged over dipole and field-free regions separately for input to the electron cloud buildup modeling.

Superposition of 300 Geant4 photon absorption events

$E_\gamma = 30$ eV

5-degree grazing angle

$E_\gamma = 2000$ eV

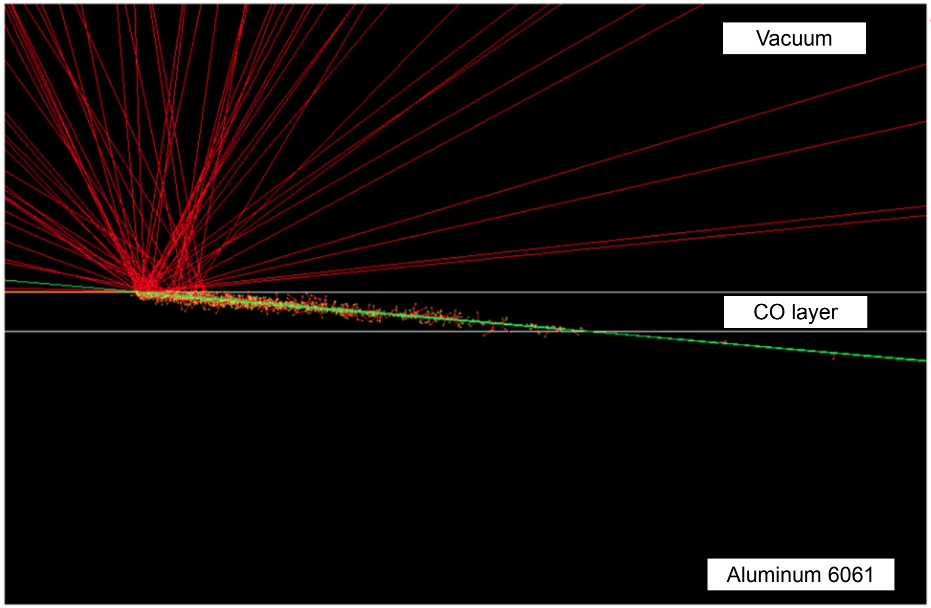

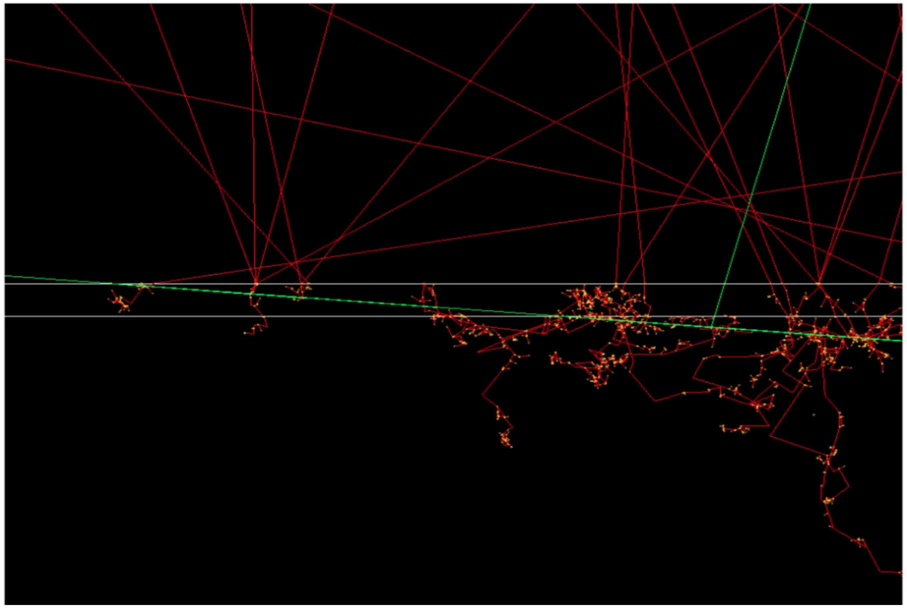

Zoom in on the 5-nm CO layer.
Low-energy photons interact predominantly in the CO layer.
High energy photons are absorbed most frequently in the aluminum

Two classes of final-state electrons can be distinguished: 1) photoproduced electrons with momenta which "remember" that of the photon. These enter the vacuum chamber at low energy via multiple scattering, and 2) electrons produced via atomi-de-excitation. These are emitted symmetrically and can carry high energy, i.e. the energy corresponding to the difference of atomic binding energy levels.

Multipole content of transfer functions using Bmad particle tracking through field maps

Multipole analysis of field map tracking for transfer matrix element R_{21}

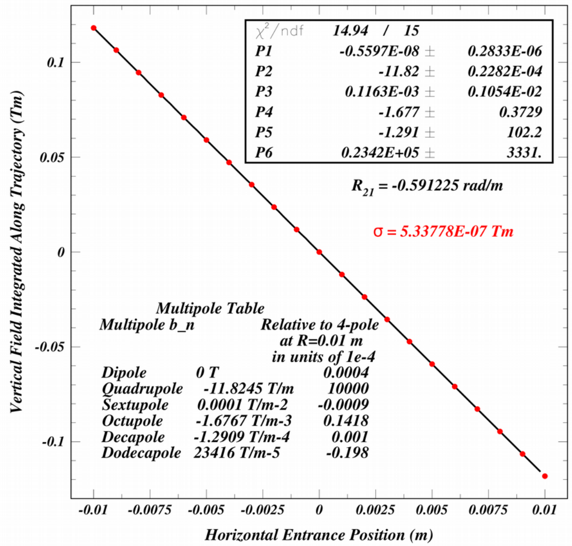

Multipole analysis of R_{21} from tracking in simple single element model for the non-extraction (symmetric) quad, defined only by a field gradient and a length. The fit is to the horizontal entrance position dependence of the exit horizontal angle expressed as the trajectory-integrated vertical magnetic field component. This is the model used in the CESR operations and development lattice now in use.

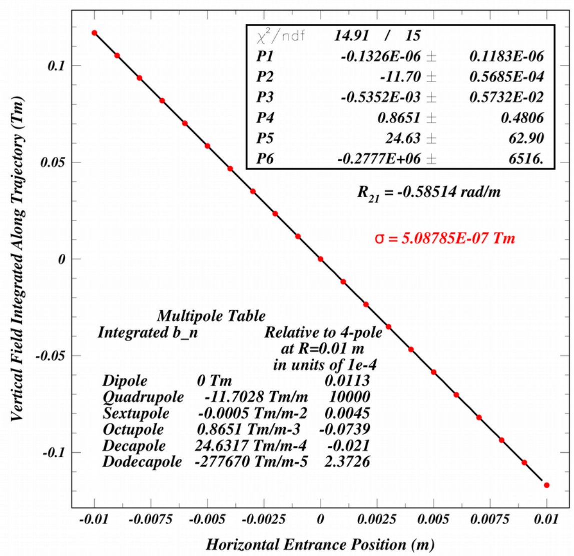

Multipole analysis of Runge-Kutta tracking in the finite-element Opera model field map. This is the most accurate and computationally slowest method to obtain the matrix elements.

A dodecapole term is found which is an order of magnitude larger than that found in the simple model above presently in use.

J.C. and S.Wang, *Comparison of Transfer Map Derivation Methods for Static Magnetic Fields*, MOPAB25, IP AC21

Offline kick analysis of orbit and phase difference measurements

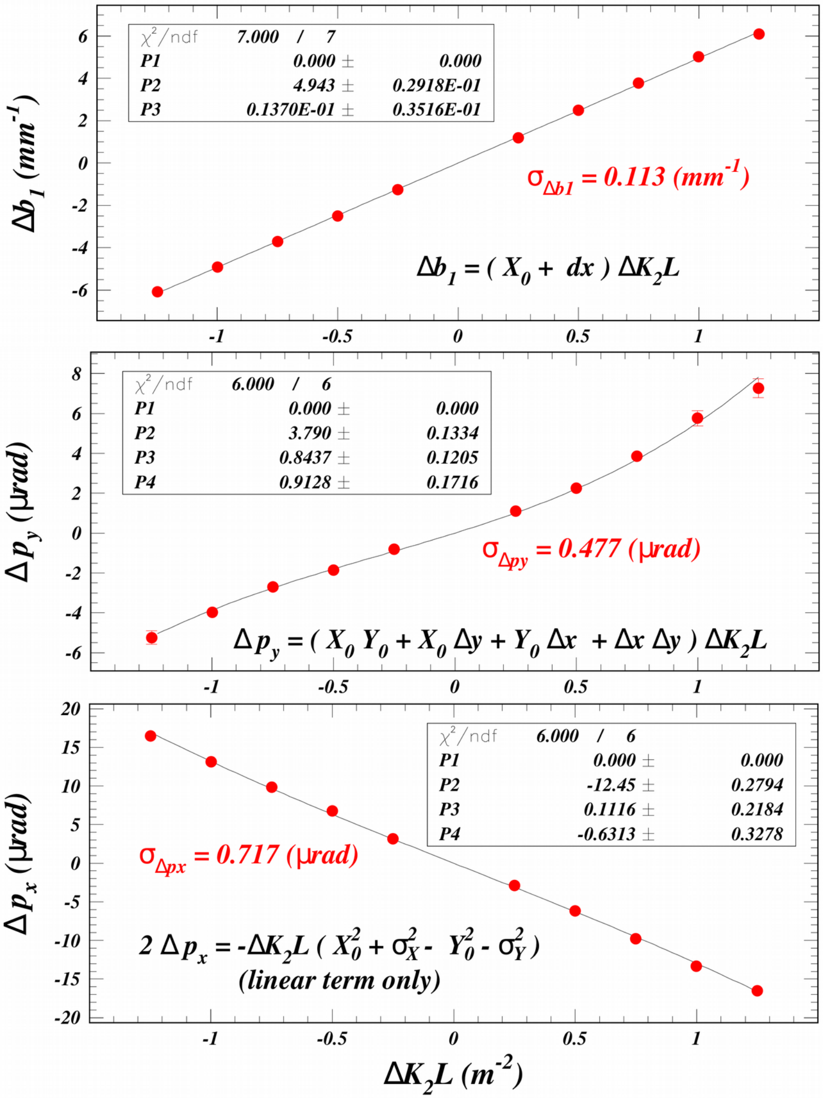

J.C.et al, *Progress on the Measurement of Beam Size Using Sextupole Magnets, MOPOTK040, IPAC22*

Record phase and orbit measurements for eleven sextupole settings. Reference the ten sets of measurements with nonzero K_2 settings to the K_2=0 orbit and phase measurements. Fit for the linear terms in $\Delta b_1(\Delta k_2 l)$, $\Delta x'(\Delta k_2 l)$, $\Delta y'(\Delta dk_2 l)$.

We obtain an estimate for the measurement uncertainties in Δb_1, $\Delta x'$ and $\Delta y'$ by setting them such that the λ^2/NDF is unity.

The linear term for Δb_1 gives the initial horizontal position of the beam relative to the sextupole center.

$$X_0 = 4.943 \pm 0.029 \text{ mm}$$

The linear term for Δp_y gives the initial value for the product of horizontal and vertical beam positions relative to the sextupole center.

$$X_0 Y_0 = 3.79 \pm 0.13 \text{ mm}^2$$

From this we obtain

$$Y_0 = 0.766 \pm 0.26 \text{ mm}$$

The linear term for Δp_x ($-12.45 \pm 0.28\times10^{-6}$ rad/m^{-2}) can be used to calculate the value

$$\sigma_x^2 - \sigma_y^2 = 1.03 \pm 0.53 \text{ mm}^2.$$

The vertical beam size is typically 20x smaller than the horizontal, so we can deduce with good accuracy

$$\sigma_x = 1.01 \pm 0.26 \text{ mm}$$

Sextupole calibration and alignment: CesrV operations script and offline analysis

Example of tune change versus beam position strategy

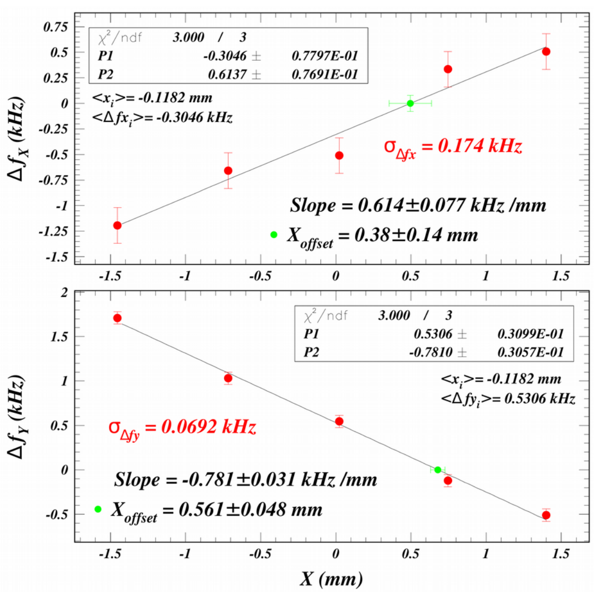

Calibration correction factor measurements and reproducibility for 76 sextupoles

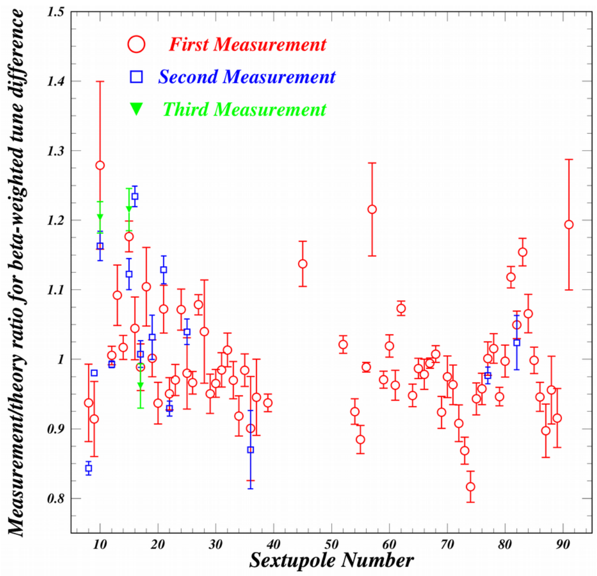

Sextupole offset measurements and reproducibility for 76 sextupoles

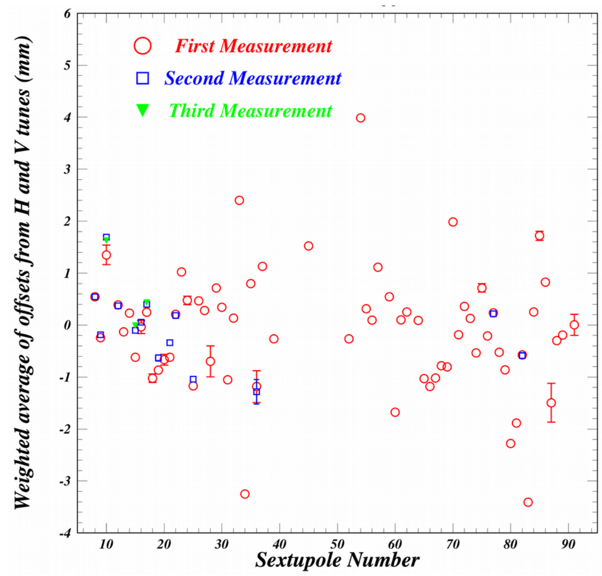

J.C. et al, *Progress on the Measurement of Beam Size Using Sextupole Magnets, MOPOTK040, IPAC22*